Discovery of Potent Thermolysin Inhibitors Using Structure Based Virtual Screening and Binding Assays

Mahmud Tareq Hassan Khan,[†,§] Ole-Martin Fuskevåg,[‡] and Ingebrigt Sylte*[,†]

Department of Pharmacology, Institute of Medical Biology, Faculty of Medicine, University of Tromsø, N-9037, Tromsø, Norway, and Department of Clinical Pharmacology, University Hospital of Northern-Norway, N-9037, Tromsø, Norway

Received July 3, 2008

In the present work, 22 compounds of the U.S. NCI compound library (size 273K) were identified as putative thermolysin binders by structure based virtual screening with the ICM software (ICM-VLS). In vitro competitive binding assays confirmed that 12 were thermolysin binders. Thermolysin binding modes of the 12 compounds were studied by docking using ICM and Molegro Virtual Docker (MVD). The most potent inhibitor had an IC_{50} value of 6.4×10^{-8} mM (NSC250686, 1β-D-arabinofuranosyl-N^4-lauroylcytosine). The structure of this compound is quite different from the other 11 compounds. Nine out of the 12 compounds contained a similar chemical skeleton (3-nitrobenzamide derivatives) and have IC_{50} values ranging from 697.48 to 0.047 mM. The ICM-VLS score and the activity profiles (pIC_{50} values) were compared and found to be somewhat linearly correlated ($R^2 = 0.78$). Kinetic studies showed that, except for NSC285166 (oxyquinoline), the compounds are competitive thermolysin inhibitors.

Introduction

Thermolysin (EC 3.4.24.27) is a secreted eubacterial endoproteinase from *Bacillus thermoproteolyticus*. Thermolysin is a 34.6 kDa bacterial Zn metalloprotease and the prototype of the M4 family of proteinases. The 3D structure contains a single catalytic zinc[1] ion essential for hydrolytic activity and four calcium[2] ions required for thermostability.[1] The enzyme catalyzes specifically the hydrolysis of peptide bonds containing hydrophobic amino acid residues.[3,4]

Most of the M4 family (thermolysin family) members are virulence factors secreted from Gram-positive or Gram-negative bacteria degrading extracellular proteins and peptides for bacterial nutrition prior to sporulation. The thermolysin family includes enzymes from pathogens such as *Legionella, Listeeria, Clostridium, Staphyloccus, Pseudomonas* and *Vibrio*. Several members of the thermolysin family are key factors in the pathogenesis of various diseases, including several types of bacterial infections,[5−7] cholera,[8] gastritis and peptic ulcer,[9,10] and gastric carcinoma.[11] Enzymes of the M4 family are important for suppressing or avoiding the innate immune system of the infected host during pathogenesis.[5,12−17] Therapeutic inhibition of enzyme of the thermolysin family is therefore believed to be a novel strategy in the development of second-generation antibiotics.[18,19]

Zn metalloproteinases with close structural and functional similarities with thermolysin are often named thermolysin-like proteinases (TLPs[a]). TLPs contain the consensus sequence HExxH, which forms the zinc-containing catalytic domain.[20,21] Several TLPs are involved in the control of different physiological functions. Neprilysin (NEP) and angiotensin-converting enzyme (ACE) are TLPs involved in the control of hypertension.[22,23] Crystallographic data of thermolysin[24] and various thermolysin−inhibitor complexes were previously used to construct models NEP and ACE that guided in the design of NEP/ACE inhibitors.[25−27] The structural and functional similarities between thermolysin, NEP and ACE indicate that thermolysin inhibitors also may inhibit ACE and NEP and be putative antihypertensives.

During past years several articles have discussed the utilities of virtual high throughput screening (vHTS) in drug discovery.[12,28−45] The importance of vHTS in drug discovery has increased simultaneously with the rapidly growing number of small molecules available in corporate and public libraries.[46] A very good number of these reports used the ICM VLS modules for their discovery initiatives.[47−54] But up to now, only one scientific paper has reported vHTS against Zn metalloprotease (matrix metalloprotease 3, MMP-3)[49] and none against thermolysin or TLPs.

In the present study in silico approaches, including target-based vHTS and docking calculations using different algorithms, were used to identify putative thermolysin inhibitors. The vHTS hits were tested by in vitro binding assays.

Results and Discussion

M4 family members and other TLPs are potential targets for therapeutic intervention. On the basis of structural and functional similarities, thermolysin may serve as a model system to identify inhibitor interactions with the active site of other TLPs and thereby for discovery of potential antibacterial or antihypertensive drugs. Computational approaches including docking and scoring, vHTS, and molecular dynamics based methods for ligand−protein affinity predictions have become integral parts of drug discovery processes. Such methods complement experimental binding affinity analysis by adding molecular insight into the binding affinities. Increased computer power and improved algorithms are important reasons for the increased use of computational approaches. However, the most important reason is the growth in available 3D structures of drug target

* To whom correspondence should be addressed. Phone: +77644705. Fax: +77645310. E-mail: sylte@fagmed.uit.no.

† University of Tromsø.

§ M.T.H.K. is a Fellow of the "Ph.D. School in Molecular and Structural Biology" at the University of Tromsø, Norway.

‡ University Hospital of Northern-Norway.

[a] Abbreviations used: ACE, angiotensin converting enzyme; DE, differential evolution; EA, evolutionary algorithm; EC, Enzyme Commission; FAGLA, *N*-[3-(2-furyl)acryloyl]glycyl-L-leucinamide; GA, genetic algorithms; ICM, internal coordinate mechanics; ICM-VLS, internal coordinate mechanics virtual ligand screening; LBP, ligand-binding pocket; LE, ligand efficiency; MDR, multidrug resistance; MMP, matrix metalloprotease; MVD, Molegro Virtual Docker; NEP, neprilysin; PDB, Protein Data Bank; PLP, piecewise linear potential; Ro5, rule of five; TLP, thermolysin-like proteinase; TMN, thermolysin; TIE, total interaction energy; vHTS, virtual high-throughput screening; VLS, virtual ligand/library screening.

10.1021/jm8008019 CCC: $40.75
Published on Web 12/15/2008

Table 1. NCI Codes, ICM-VLS Scores, and Activity Status of the 21 VLS Hits

compd	NSC code (NCI)	ICM-VLS score	status[a]
1	239336	−43.8903	*b*
2	82028	−24.7355	A
3	79459	−30.1023	A
4	79456	−25.9124	A
5	241514	−23.3793	IA
6	82020	−22.3550	A
7	82019	−34.8770	A
8	250684	−20.7766	LA
9	250686	−59.2232	A
10	201290	−19.1524	IA
11	313985	−12.8474	IA
12	313981	−8.39318	IA
13	107876	−30.1964	A
14	309546	−7.78814	IA
16	285166	−43.2655	A
17	82029	−42.6830	A
18	79451	−13.7203	*b*
19	90411	−39.2355	A
20	82024	−46.0381	A
21	82025	−41.9239	A
22	79453	−20.9182	*b*

[a] "Status" means experimentally active or not. A = active. LA = less active, not possible to calculate the IC_{50} values. IA = inactive. [b] Compound not received from NCI. Compund **15** was removed after MS analysis due to lack of purity.

proteins, which has given the possibility of predicting binders using computational methods early in the drug development phase. In the present study a combination of computational methods and experimental approaches was used to discover thermolysin inhibitors and gain structural insight into their mode of binding.

ICM-Structure Based Virtual Ligand Screening. In order to reduce CPU time for screening, the number of compounds was reduced. Large size molecules and molecules containing unusual heteroatoms were excluded, while others were excluded based on Lipinski rule-of-five (Ro5).[55] Finally, 1170 compounds from the 273K compound library of NCI were being screened by ICM virtual ligand screening (ICM-VLS). The nature of the active site is important for the speed of the ICM-VLS process. Thermolysin has a Zn ion at the active site. Our experiences are that presence of metal ion at the active site reduces the speed of the ICM-VLS process (unpublished data).

On the basis of the ICM-VLS score, 19 compounds (obtained from Drug Synthesis and Chemistry Branch, DTP, Division of Cancer Treatment and Diagnosis, NCI) were finally taken in considerations for in vitro studies using competitive binding assays. Compound **15** was inititally tested, but removed from further testing after MS analysis. The number of experimentally positive hits was 12 (66.67%) and the remaining 6 were false positive hits, giving a percent of false positive hits of 33.33. The percent of experimental hits when considering the entire NCI library was about 0.004% before filtering and 1.03% after the filtering process. These results also show the necessity of filtration, which increases the speed and reduces the number of false positives. Table 1 presents compound code numbers, NCI codes, ICM-VLS scores, activity status after experimental testing of the VLS hits, and the identification codes used in the present study.

Experimental IC_{50} values (in mM) of the 12 compounds confirmed by competitive binding assays as thermolysin binders together with some of their chemical features are shown in Table 2. Molecular structures of the compounds are shown in Figure 1.

Structure-based virtual screening algorithms, like ICM-VLS, contain a docking procedure that generates hypothetic interaction mode(s) and a scoring procedure that evaluates the binding modes and assigns scores, which finally is employed to rank the ligands according to the quality of their fits to the target, ideally reflecting the affinity of binding.[54] During the ICM-VLS processes different scorings were considered. One of them was ICM-VLS, which is a fast potential and empirically adjusted scoring (Table 1) that includes a solvation electrostatic free energy term calculated by the REBEL algorithm.[64] Other scorings calculated were mfScore (potential of mean force score), hydrogen bonding energy, and hydrophobic energy. The scores for the 12 experimentally verified hits are shown in Table 3, together with their activity profiles (pIC_{50} values). The binding mode of compound **9** (the most potent compound) suggested by the ICM-VLS process is shown in Figure 2.

ICM-VLS Scoring vs in Vitro Results. The experimental activity profiles (IC_{50} values) were compared with the scoring values obtained by the ICM-VLS process using linear regression analysis. Figure 3 indicates that the ICM-VLS scores (Table 1) were most linearly related to the experimental pIC_{50} ($-\log IC_{50}$) values ($R^2 = 0.78$). For the other scoring values, their regression coefficients (R^2) were less than 0.6 (statistically insignificant), indicating that they did not reproduce the relative ranking of the experimental observations. Therefore, Figure 3 indicates that ICM-VLS score was more useful than mfScore (potential of mean force score), Hbond (hydrogen bonding energy), and Hphob (hydrophobic interaction energy) for predicting thermolysin inhibitors.

Except for compounds **9**, **13**, and **16** all compounds confirmed as thermolysin binders (Table 3) contain a common structural skeleton consisting of an amid group connected to 2-hydroxy-3-nitrobenzene group and a benzene ring with varying functional substituents (methyl, ethyl, bromide, chloride, methoxy, nitro). This structural skeleton is indicated in Figure 4 where the compounds (Figure 1) containing the skeleton are superimposed. The thermolysin binders were further studied by enzyme kinetics and docking.

Kinetic Analyses. Enzyme kinetic were performed using Lineweaver−Burk, Michaelis−Menten, and Dixon−Hill methods. The results of enzyme kinetics studies are shown in Table 4. These studies indicated that all compounds, except for compound **16**, are competitive inhibitors. Double reciprocal (1/[FAGLA] in mM vs 1/reaction rate, *V*, in (mmol/min)/mg) Lineweaver−Burk plots of some of inhibitors are shown in Figure 5.

Time dependent enzyme−inhibitor reaction kinetics showed that at inhibitor concentrations of 50 μM most of the compounds still bound after 2 h of reaction (Figure 6). This may indicate that they are "slow binders" with high affinity for thermolysin. Similar trends were also observed in previous reports.[68−70] Two phosphonamidate peptide inhibitors, carbobenzoxy-Gly^P-L-Leu-L-Leu (ZG^{P}LL) and carbobenzoxy-L-Phe^P-L-Leu-L-Ala(ZF^{P}LA) with very strong inhibitory (K_i values of 9.1 and 0.068 nM, respectively) potentials to thermolysin showed slow binding during the complexation process.[69] This is often attributed to the rapid formation of an enzyme−inhibitor complex followed by a slow conformational isomerization to a tight complex.[71−73] The observation that thermolysin had essentially the same conformation in the absence of inhibitors and in complexes with slow or faster binding inhibitors ruled out mechanisms in which the enzyme undergoes a substantial conformational change during binding.[69]

Docking Calculations. In order to study the binding modes of the 12 compounds identified as thermolysin binders, docking calculations were performed using ICM and Molegro Virtual

Table 2. Experimental IC_{50} Values of VLS Hits Indentified as Thermolysin Inhibitors, Compound Code Numbers Used in the Present Study, Chemical Features (Chemical Names, Molecular Formula, Molecular Weight), and CAS Number[a]

compd	CAS no.	chemical name	mol. formula	MW	IC_{50} values (mM)	ref
2	73454-96-3	*N*-(2,3-dimethylphenyl)-2-hydroxy-3-nitro-benzamide	$C_{15}H_{14}N_2O_4$	286	294.06	56
3	33581-05-4	*N*-(5-chloro-2-methoxyphenyl)-2-hydroxy-3-nitro-benzamide	$C_{14}H_{11}ClN_2O_5$	323	81.41	57
4	33581-08-7	*N*-(2,4-dimethylphenyl)-2-hydroxy-3-nitro-benzamide	$C_{15}H_{14}N_2O_4$	286	161.14	57
6	33580-97-1	*N*-(2-chloro-4-nitrophenyl)-2-hydroxy-3-nitro-benzamide	$C_{13}H_8ClN_3O_6$	338	697.48	58
7	33580-95-9	5-bromo-*N*-(4-bromophenyl)-2-hydroxy-3-nitro-benzamide	$C_{13}H_8Br_2N_2O_4$	416	48.13	59
9	55726-42-6	1β-D-arabinofuranosyl-N^4-lauroylcytosine	$C_{21}H_{35}N_3O_6$	426	6.4×10^{-08}	60
13	30932-95-7	not found at source	$C_{14}H_{22}O_2$	222	91.57	61
16	148-24-3	oxyquinoline or quinophenol	C_9H_7NO	145	0.35	62
17	63981-16-8	*N*-(2,5-dimethylphenyl)-2-hydroxy-3-nitrobenzamide	$C_{15}H_{14}N_2O_4$	286	14.54	
19	73454-91-8	*N*-(2-ethylphenyl)-2-hydroxy-3-nitrobenzamide	$C_{15}H_{14}N_2O_4$	286	29.5	63
20	73544-89-5	*N*-(2-chloro-6-methylphenyl)-2-hydroxy-3-nitrobenzamide	$C_{14}H_{11}ClN_2O_4$	307	0.047	
21	73454-90-7	2-hydroxy-*N*-(4-methyl-2-nitrophenyl)-3-nitrobenzamide	$C_{14}H_{11}N_3O_6$	317	20.58	

[a] Source for chemical features is http://dtp.nci.nih.gov/dtpstandard/ChemData/index.jsp, and the references of the compounds citations are from SciFinder Scholar.

Table 3. Experimental (pIC_{50}, $-\log IC_{50}$) Values and Scores Obtained by Different Scoring Algorithms of Positive VLS Hits[a]

compd	pIC_{50}	ICM-VLS score	mfScore	Hbond	Hphob
2	−2.4684360	−24.7355	−49.8417	−1.23229	−4.37299
3	−1.9106778	−30.1023	−77.6134	−2.88318	−4.79094
4	−2.2072034	−25.9124	−55.1310	−1.24014	−5.14992
6	−2.8435318	−22.3550	−41.5040	−1.23352	−4.50400
7	−1.6824159	−34.8770	−53.4101	−1.27285	−5.09298
9	7.19382003	−59.2232	−153.290	−6.69245	−6.57258
13	−1.9617532	−30.1964	−105.182	−3.30275	−5.85623
16	0.45593196	−43.2655	−47.9014	−3.67542	−3.38986
17	−1.1625644	−42.6830	−39.2669	−2.91399	−4.83127
19	−1.4698220	−39.2355	−36.5526	−3.04642	−4.72559
20	1.32790214	−46.0381	−52.9612	−3.57504	−4.48770
21	−1.3134454	−41.9239	−48.1556	−3.50110	−4.17856

[a] ICM-VLS score: ICM virtual ligand screening score. mfScore: potential of mean force score. Hbond: hydrogen bonding energy. Hphob: hydrophobic interaction energy. The values are in kcal/mol.

Docker (MVD). For each compound a stack of docked complexes with different ligand conformations and orientations was generated. The most realistic complex of each compound was selected on the basis of docking energy ($E_{docking}$) and similarities with known X-ray crystal structure complexes of thermolysin (hydrogen bonding interactions with amino acids in thermolysin and Zn interactions). The thermolysin binding energy (BE) was calculated for the most realistic complex of each compound using the ICM "calcBinding energy" script. ICM was also used to dock four compounds with known X-ray crystal structure in complex with thermolysin (PDB codes 2TMN, 3TMN, 1TLP, and 1GXW). The root-mean-square deviation (rmsd) between the best docking poses and X-ray crystal structures were 2TMN 0.26 Å, 3TMN 0.27 Å, 1TLP 0.27 Å, and 1GXW 0.01 Å. However, calculated BE values were overestimated compared with ΔG calculated from experimental inhibition constants. On the basis of these docking studies, it seems that ICM performs well in reproducing experimental binding modes of thermolysin complexes. Insufficient zinc parametrization and the fact that we used a formal charge of +2 for zinc may have contributed to the overestimation.

Linear regression analyses of $E_{docking}$ and BE values against experimental K_i values (pK_i) of the 12 thermolysin binders of the U.S. NCI compound library showed that BE was significantly correlated with pK_i, as the regression coefficient R^2 was 0.744, while the correlation with $E_{docking}$ was less significant ($R^2 = 0.66$). The scatter plots are shown in Figure 7.

The experimental K_i (pK_i) values were also compared with different scores from MVD (Table 5) using linear regression analysis. Interestingly, these scores were correlated to experimental binding affinities (Figure 8); in particular, predicted binding affinities (affinity, Table 5) were highly correlated ($R^2 = 0.875$). Three other scores also showed correlations in the same range with the experimental affinities (MVDscore, $R^2 = 0.827$; TIE, $R^2 = 0.9443$; and docking score, $R^2 = 0.7023$). The different scores are explained in the methods section.

Protein−Inhibitors Interactions. Main protein−inhibitors interactions (hydrogen bonding and zinc interactions) are given in Table 6. The molecular interactions of some of the compounds (**4**, **7**, **16**, **17**, **19**, and **21**) with thermolysin are also shown in Figure 9.

The docking poses obtained by ICM and MVD docking were very similar. Except for compound **9**, the rmsd between the best raked pose of the ICM and MVD docking was 0.1−0.15 Å for all inhibitors. Compound **9** has a very flexible aliphatic side chain which contributes to an rmsd of 2.4 Å between the best ranked ICM- and MVD-docking pose. In the following the hydrophobic interactions of the highest ranked docking poses are described.

Atoms C6 and C11 of compound **2** (Figure 1) had hydrophobic interactions with His146. Atom C7 interacted with His231, while C9, C14, C15, C18, and C19 interacted with His142. C13 interacted with Ala113, while C18 interacted with Phe130, Leu133, and Val139.

Atom C1 in **3** (Figure 1) had hydrophobic interactions with Glu143 and Val139, while C6 had hydrophobic interactions with the following amino acids: Val139, Phe114, Glu166, Tyr157, His146, and His231. In addition the following interactions of N03 were seen: C7 with Tyr157, Glu166, and Phe114; C9 with Asn112; C11 with Glu166, Tyr157, and His146; C12 with Glu166 and Phe114; C14 with Val139 and Leu133; C15 with Asn112, Val139, Glu143, and Leu133; C17 with Tyr157; C18 with Ile188, His142, and His231; C19 with Glu143 and Leu202.

Atoms C1, C12, C13, and C17 of **4** (Figure 1) had hydrophobic interactions with His231 and Leu202. C6 (Figure 1) interacted with His142 and Asn113. C9 and C15 interacted with His146, and atom C15 interacted with Leu202 (Figure 9).

Atom C10 of N06 (Figure 1) had hydrophobic interaction with His231. In addition the following interactions were observed: C9, C14, and C15 with His146 and Phe114, C11, C12, and C17 with His146 and Leu202.

Atom C6 of **7** (Figure 1) had hydrophobic interacts with His142, His146, and Tyr157. C9, C13, and C14 exhibited hydrophobic interactions with His146, as well as with Phe114 and Tyr157. Atom C12 interacted with Asn113 (Figure 9).

Atom C4 of **9** (Figure 1) had hydrophobic interactions with Asn112, Val139, and Leu202. Atom C9 showed interactions with Asn112, Leu133, and Glu143, and atoms C10 and C14

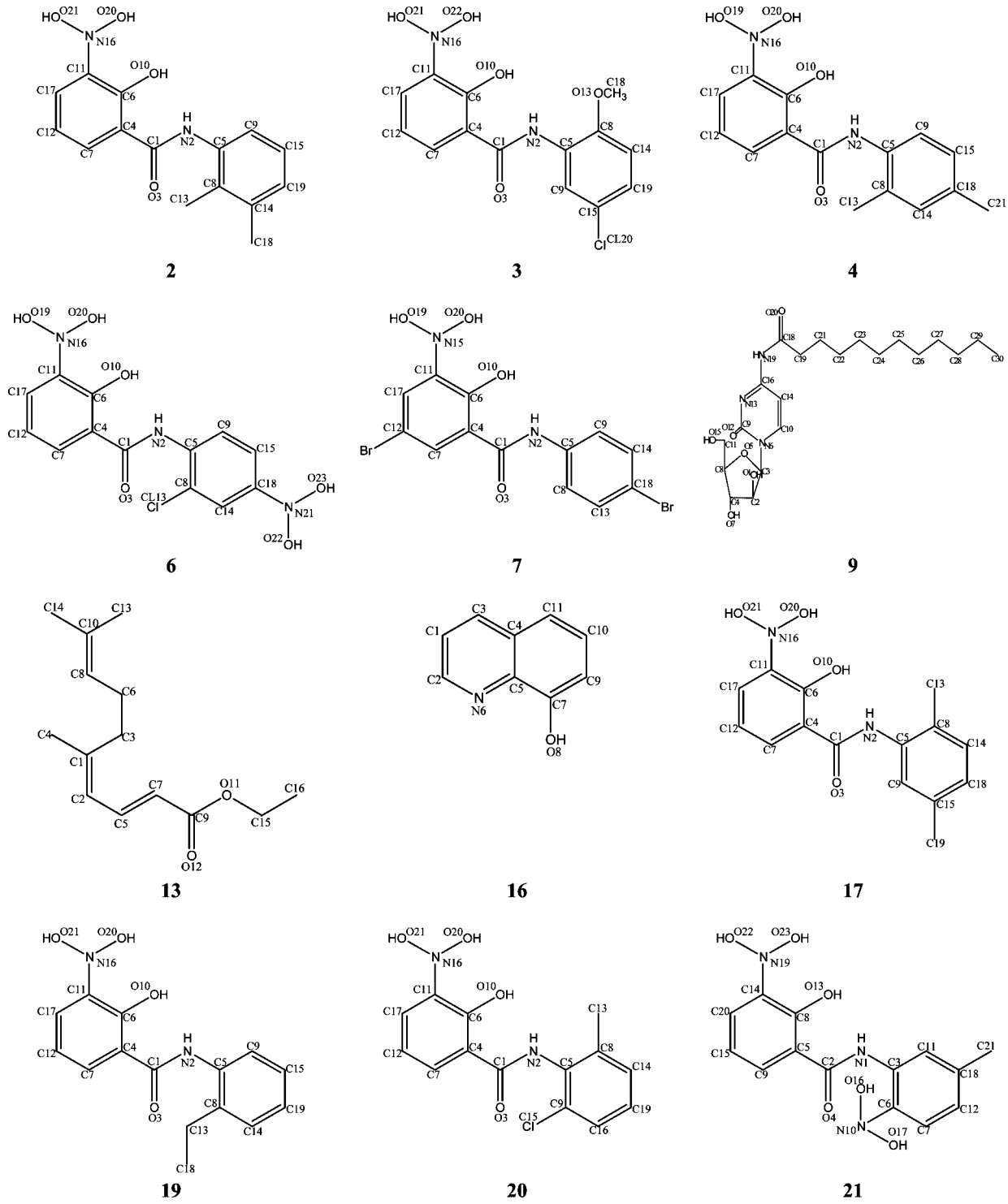

Figure 1. Molecular structures of confirmed thermolysin binders. Atom numbering assigned by the ICM program is indicated.

interacted with His146. C14, C18, and C22 interacted with Tyr157. C22 interacted with Gly117, and C24, C26, C27, C28, and C29 interacted with Asp150.

Atoms C2, C3, C7, and C8 of compound **13** had hydrophobic interactions with Phe114. C7 and C16 had hydrophobic interactions with the His146. Atoms C8, C10, and C13 interacted with Tyr157, while atoms C15 and C6 interacted with Glu143, His142, Ile188, and Leu202.

C1, C3, C4, and C10 of **16** (Figure 1) had hydrophobic interactions with Asn112. C2, C3, and C10 interacted with Leu202, and C7 had weak interactions with His142 (Figure 9).

C1 and C13 of **17** (Figure 1) had hydrophobic interactions with His231. In addition, the following interactions were seen: C6, C7, and C11 with His142; C6 with Asn112; C9 and C19 with His146 and Tyr157; C12 and C17 with Leu202; C14 and C15 with Phe114; and C15 with His146 (Figure 9).

C1, C13, and C18 of **19** showed hydrophobic interactions with His231. In addition, atoms C9, C14, and C15 interacted with Phe114 and His146, and C6 interacted with His142 and His146. C7 had hydrophobic interaction with Asn112, C11 with His142, and C12 and C17 had hydrophobic contacts with Leu202 (Figure 9).

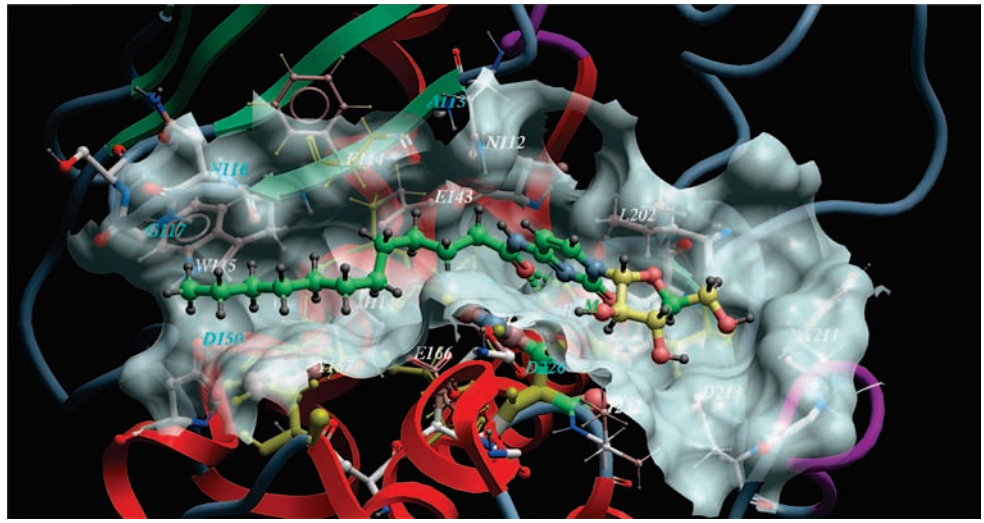

Figure 2. Interaction mode of compound **9** (ball and stick model) suggested by the ICM-VLS procedure. The carbon atoms of **9** are shown in light-green, hydrogen atoms in gray, oxygen atoms in pink, and nitrogen atoms in purple. Side chain sugar moiety is shown in yellow.

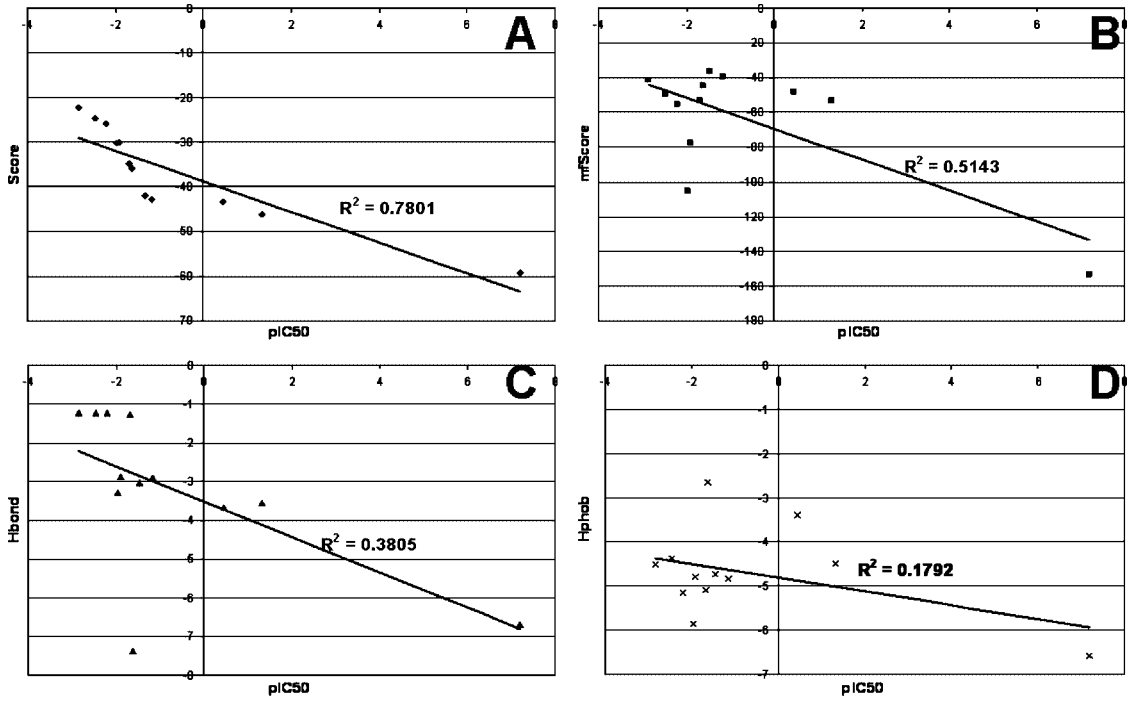

Figure 3. Scatter plots of the in vitro activity profiles (pIC_{50} values) vs scores of the thermolysin binders of the NCI compounds, where the linear relationship between the activity profiles and the ICM-VLS scores showed the best correlation (A). Panels B, C, and D show the correlation between the activity profiles and mfScore (B), energy of hydrogen bonding (C), and energy of hydrophobic interactions (D).

Atom C6 in **20** (Figure 1) demonstrated hydrophobic interactions with Phe114 and Tyr157. In addition, the following interactions were seen: atoms C7 and C12 interacted with His231 and Glu166, C9 with Leu202 and Val139, C11 with His146, C14 with Val139 and Leu133, C13 with His142, C16 and C19 with Leu202, C16 with Val139, and C18 had hydrophobic interactions with Glu166, Tyr157, and Phe114.

C8 and C14 of **21** (Figure 1) revealed hydrophobic interactions with the active site residue His146. In addition C12 and C18 interacted with Leu202, C21 with Asn112 and Leu133 (Figure 9).

X-ray crystallographic structures of thermolysin in complex with inhibitors show that all inhibitors contain carboxyl acid, hydroxamide, sulfydryl, dialkylsilanediol, or phosphinic groups that form bidentate or monodentate arrangements with the catalytic zinc. The experimentally confirmed binders in the present study (Figure 1) contain carbonyl, amide, or hydroxyl groups that may form arrangements with zinc similar to those observed in the X-ray crystal structure complexes. The highest scored docking poses indicated that compounds **9**, **13**, and **20** did not interact with zinc while compounds **2**, **6**, and **16** interacted rather distantly with catalytic zinc. The other compounds formed at least one strong interaction with zinc (Table 6). Interestingly, the putative zinc binding groups of compound **9**, which seems to be a potent thermolysin inhibitor, did not interact with the catalytic zinc. Figure 10 shows the superimposition of the docked complex of compound **9** (most potent inhibitor in the present study) and the X-ray complex of the inhibitor *N*-phosphoryl-L-leucinamide (PDB code 1tlp).[75] The two ligands are relatively different in structure. The inhibitor of the X-ray structure interacts within the S1, S1′, and S2′ pockets of thermolysin with an oxygen of the phosphoramide moiety coordinating zinc. Compound **9** contains carbonyl, hydroxyl, and amide groups that putatively could form interac-

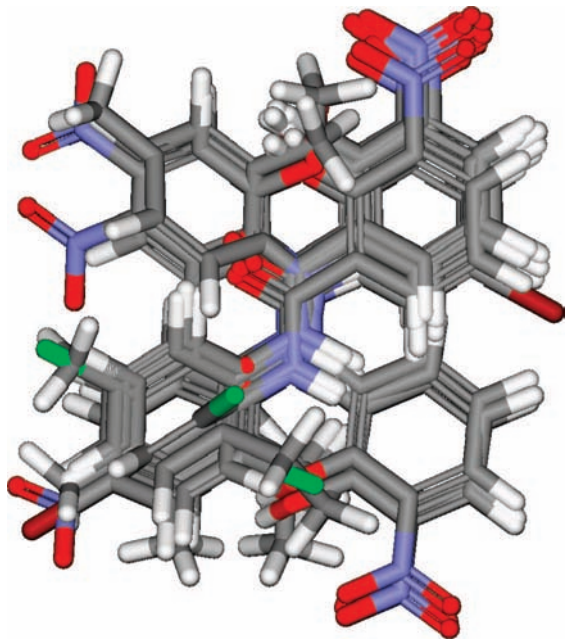

Figure 4. Superimposed stick models of the structures of **2**, **3**, **4**, **6**, **7**, **17**, **19**, **20**, and **21**, showing that they all share a common molecular skeleton. Carbon atoms of the main skeleton are shown in gray, oxygen atoms in red, hydrogens in white, chlorine atoms in green, and nitrogen atoms in blue.

Table 4. Enzyme Kinetic Data of Thermolysin Binders[a]

compd	V_{max} ((mmol/min)/mg)	K_m (mM)	K_i (mM)
2	1.155×10^5	2.195×10^5	2.94×10^2
3	71.91×10^3	1.332×10^5	8.14
4	4.720×10^5	9.512×10^5	1.61×10^2
6	4.284×10^5	8.703×10^5	6.97×10^2
7	2.809×10^5	5.932×10^5	4.81
9	3.692×10^5	7.242×10^5	6.40×10^{-8}
13	0.282×10^5	0.57×10^5	9.16
16	1.3047	1.5764	0.214
17	0.986×10^5	2.791×10^5	1.45
19	3.249×10^5	9.842×10^5	2.95
20	2.994×10^5	9.096×10^5	4.70×10^{-2}
21	5.493×10^5	1.124×10^6	2.06

[a] V_{max} and K_m were directly derived from the kinetic experiments, and the K_i values were determined from IC_{50} values using the Cheng−Prusoff relationship.[65−67]

tions with catalytic zinc. However, Figure 10 indicates that these groups did not form interactions with zinc. The ring system of compound **9** interacted with amino acids within the S1′ and S2′ pockets of thermolysin. Two hydroxyl oxygens interacted with Arg203 (S1′ pocket), while the amide group interacted close to His146, Tyr157, and His231. This observation is based on theoretical studies only and should be further examined experimentally. Table 6 and Figure 9 indicate that several of the compounds interacted with zinc via their amide and/or hydroxyl groups similar to zinc interaction modes observed in X-ray crystal structure complexes.

The X-ray crystal structures of thermolysin show that His142, His146, and Glu166 coordinate the catalytic zinc, while Glu143 and His231 are required for the catalytic activity. Most compounds had several hydrogen bonding or hydrophobic interactions with these amino acids (Table 6, Figure 9). Therefore, the present docking indicates that thermolysin inhibitors may not need to interact directly with the catalytic zinc, but inhibition may be obtained by forming interactions with other functionally important amino acids.

Compound **16** is structurally different from the others (Figure 1) and did not have hydrogen bonding interactions with any of the amino acids involved in zinc coordination or catalytic activity. Figure 9 indicates that **16** binds thermolysin quite differently from the others, and differences in binding mode (especially the hydrogen bonding patterns) may explain why **16** is not a competitive inhibitor in contrast to the other compounds (Figure 5).

Conclusion

In the present study we have successfully demonstrated the use of computational approaches to identify thermolysin binders in a fast and inexpensive manner. Systematic structure based virtual screening of the NCI compound library using ICM-VLS identified 22 compounds as putative thermolysin binders. Twelve of these compounds were confirmed by binding assays as thermolysin inhibitors. Most of the 12 inhibitors (9 compounds) contain a common structural scaffold. However, the most potent inhibitor (compound **9**) is structurally different from the other compounds. Except for **16**, the compounds formed strong hydrogen bonding interactions and hydrophobic interactions, with central amino acids being important for zinc coordination or thermolysin activity, and in contrast to the other compounds, **16** did not seem to be a competitive inhibitor. The most potent inhibitors may also function as "leads" for developing stronger thermolysin binders. Because of structural and functional similarities between thermolysin and other TLPs, these compounds should also be tested for their binding to other TLPs like ACE and NEP.

vHTS has become essential for the discovery of lead compounds and may serve as an alternative to experimental high throughput screening in drug discovery.[76] Unfortunately there are still many obstacles present for these kinds of approaches, especially false positive hits (33.33% in this study). In spite of recent theoretical and procedural advancements in the field,[77] the vHTS methods still need improvements in handling of structural flexibility of ligands and targets[78,79] and thereby reduce the number of false positives. As the field is rapidly improving, there are hopes that these kinds of problems will also be solved by development of new and improved algorithms.

Experimental Section

Chemicals. Chemicals used for binding assays and kinetic studies were purchased from Sigma-Aldrich. Three-times crystallized thermolysin (activity ≥7000 units/mg) was from CalBioChem (E-Merck, Germany). According to the manufacture's instructions, the lyophilized protein was first reconstituted in 42% glycerol adjusted to pH 8.0 with 0.01 N NaOH, containing 0.005% Triton X-100.

In Vitro Assay. Steady-state enzyme assays were performed at 25 °C using the spectrophotometric method of Feder and Schuck.[80] A 96-well microplate was used instead of a single cuvette, thereby increasing the throughput of the experiments compared with the original method described by Feder and Schuck. The thermolysin activity was determined by following the decrease in absorption at 346 nm due to enzymatic hydrolysis of the substrate *N*-[3-(2-furyl)acryloyl]glycyl-L-leucinamide (FAGLA). Initial velocities were determined for <10% of the reaction. Stock solutions of Tris (50 mM), NaBr (2.5 M), and $CaCl_2$ (10 mM), pH 7.0, were prepared and stored at 4 °C. A stock solution of FAGLA was prepared in dimethylformamide (DMF) and diluted with buffer to a final concentration of 0.1 M Tris, 0.1 M NaBr, and 2.5 mM $CaCl_2$, pH 7.0 (final concentration of DMF, 2.5%).

The total volume of the reaction mixture was 200 μL, in a final enzyme concentration of 50 nM, and with a substrate concentration of 1.0 mM. The enzyme and compounds were incubated for 15 min at 25 °C in a temperature-regulated 96-well microplate. Initial

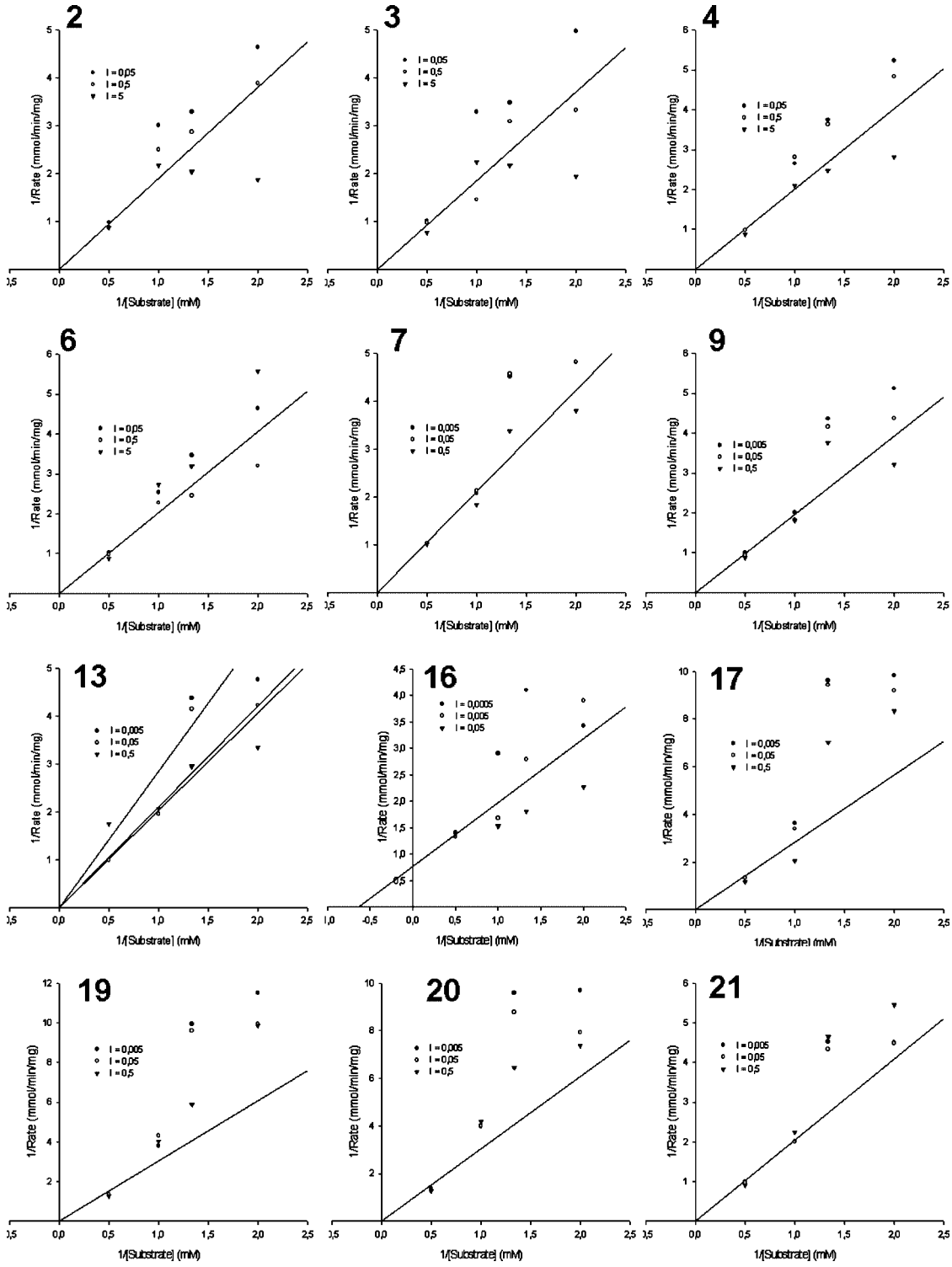

Figure 5. Double reciprocal "Lineweaver−Burk" plots of the compounds identified as thermolysin binders. *X* axis is showing 1/[FAGLA] in mM, and *Y* axis is showing 1/reaction rate, *V*, in (mmol/min)/mg.

velocities after adding the substrate were determined for <10% reaction in duplicate for each inhibitor concentration. Control (solvent) readings were taken in six replicates during each experiment. Preliminary inhibition studies were performed in duplicate at three different concentrations (0.5, 0.05, and 0.005 mM) for all compounds, and percent inhibition as well as IC_{50} values were calculated for the active compounds.

Enzyme Kinetic Studies. The enzyme kinetic studies were performed for the compounds showing prominent inhibition of thermolysin during initial inhibition studies. All methods were similar to the initial studies (described above) except that multiple concentrations of the substrate (FAGLA) were used (2, 1, 0.75, and 0.5 mM). The kinetic parameters (V_{max}, K_m) were calculated using the Enzyme Kinetic module of SigmaPlot, version 10, integrated with SigmaStat.

K_i values were determined from IC_{50} of the inhibitors values using the Cheng−Prusoff relation.[65−67]

$$K_i = IC_{50}/(1 + S/K_m) \quad (1)$$

where S is the substrate concentration.

Time Dependent Reactions. Kinetic studies were performed in order to study the association and dissociation depending on time.

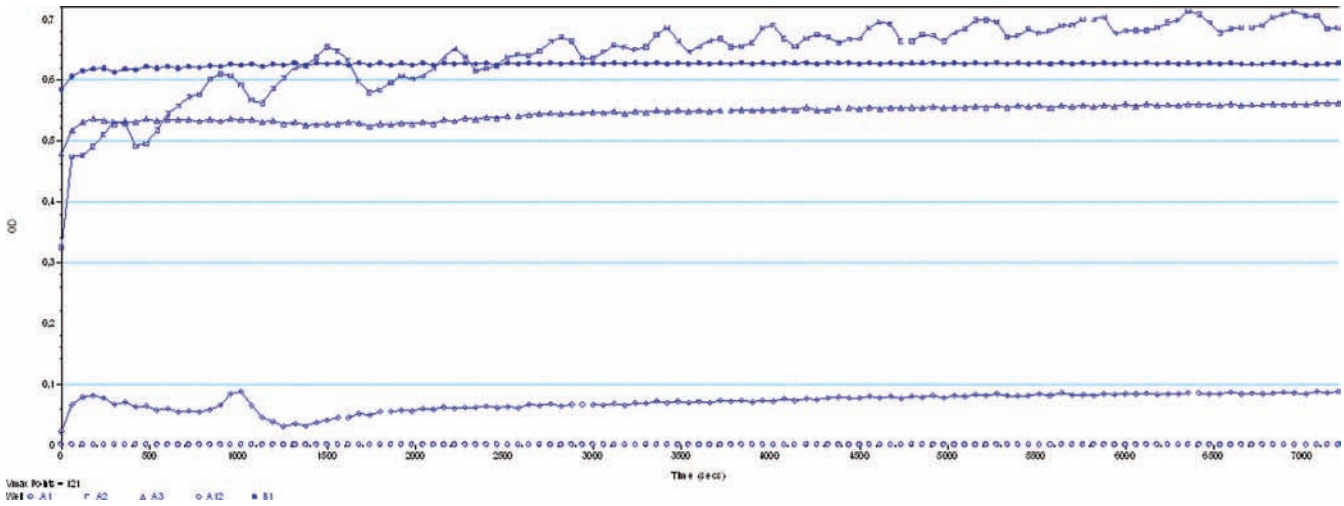

Figure 6. Time dependent enzyme−inhibitor reaction kinetics of compounds **3** (A2, unfilled square), **2** (A3, unfilled triangle), **16** (A12, unfilled rhombos), and **19** (B1, filled circle) when compared with the solvent as control (at A1, unfilled circle). Active compounds not shown in the figure were most similar to **16**: *X*-axis, time in seconds; *Y*-axis, the absorbance (optical density, OD).

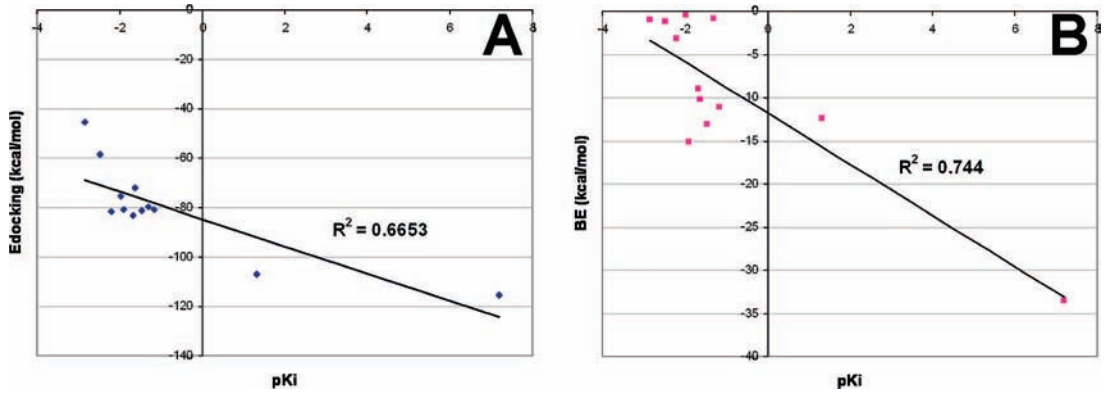

Figure 7. Scatter plots of pK_i vs (A) docking energies ($E_{docking}$, in kcal/mol) and (B) calculated binding energies (BE, in kcal/mol) from ICM docking (data are not shown in tabular form).

Table 5. Different Scores Derived from the MVD Docking Tools Compared with Experimental pK_i

compd	pK_i	MVD score	affinity (kcal/mol)	ReRank (kcal/mol)	TIE (kcal/mol)	Hbond (kcal/mol)	LE1 (kcal/mol)	LE2 (kcal/mol)	docking score
2	−2.46843	−89.4536	−2.281622274	−15.81352661	−19.9718	−2.64565	−1.01741	−0.29063	−79.233
3	−1.91067	−95.4184	−2.681688989	−17.10780812	−22.8014	−2.27005	−1.03592	−0.33903	−97.1813
4	−2.2072	−95.5725	−2.740349517	−17.91419931	−20.5243	−2.70758	−1.087	−0.28972	−81.101
6	−2.84353	−82.8569	−1.867177042	−17.20399132	−20.8727	−2.68761	−0.96428	−0.30964	−77.6549
7	−1.68242	−91.102	−3.141371615	−19.58664537	−21.3597	−2.61333	−1.13852	−0.37706	−94.539
9	7.193821	−114.228	−8.175285696	−9.0659178	−34.4559	−1.7169	−0.91212	−0.11328	−115.643
13	−1.96175	−91.94	−2.989776186	−18.13661252	−21.9772	−1.19423	−1.50681	−0.32121	−81.814
16	0.669279	−95.6783	−6.061858635	−10.89437794	−19.6909	−2.04638	−1.25238	−0.55108	−97.5693
17	−1.16256	−90.8142	−3.338491054	−16.9656471	−22.7183	−1.9698	−1.03289	−0.2751	−92.7419
19	−1.46982	−90.7237	−3.722435678	−17.36578547	−20.4168	−2.7071	−1.03191	−0.291	−92.8511
20	1.327903	−99.5722	−6.889148832	−16.64621472	−27.1181	−2.63409	−1.13249	−0.32805	−104.699
21	−1.31344	−95.4528	−4.035944675	−16.562762	−22.7589	−3.456	−0.99124	−0.27932	−97.7197

The total duration of the experiments was 2 h, giving a total of 121 data points (1 point/min).

Virtual High-Throughput Screening (vHTS). Library Preparation. Before the structure-based virtual ligand/library screening (VLS) process, the downloaded NCI library was filtered using the Lipinski rule-of-five (Ro5)[55] and manually filtered for removing very large molecules, dimers, polymers, molecules containing unusual heteroatoms, and highly reactive functional groups. Finally 1170 compounds out of the 273K compound library were used for VLS by the ICM-VLS algorithm.

Target Preparation. The target thermolysin (PDB code 1gxw[81]) was loaded into the ICM program and prepared for docking. The retrieved coordinates were converted to ICM objects. Hydrogen atoms were added and optimized using the ECEPP/3 force field of ICM. The target was optimized using Monte Carlo simulation and energy optimizations. A grid map (5 Å) that included the active site amino acids and zinc was generated.

VLS Method. A flow scheme indicating the steps of the VLS process is shown in Figure 11. The modified NCI library (1170 compounds) was screened against the prepared target using the ICM-VLS algorithm (version 3.4) according to the descriptions in the ICM manual.[64,82−84] Grid potentials were rapidly generated which accounted for shape of the binding pocket, hydrophobicity, electrostatic potentials, and hydrogen-bonding profile. The compounds were automatically screened for their putative thermolysin binding properties using a rigid target and flexible ligands in the

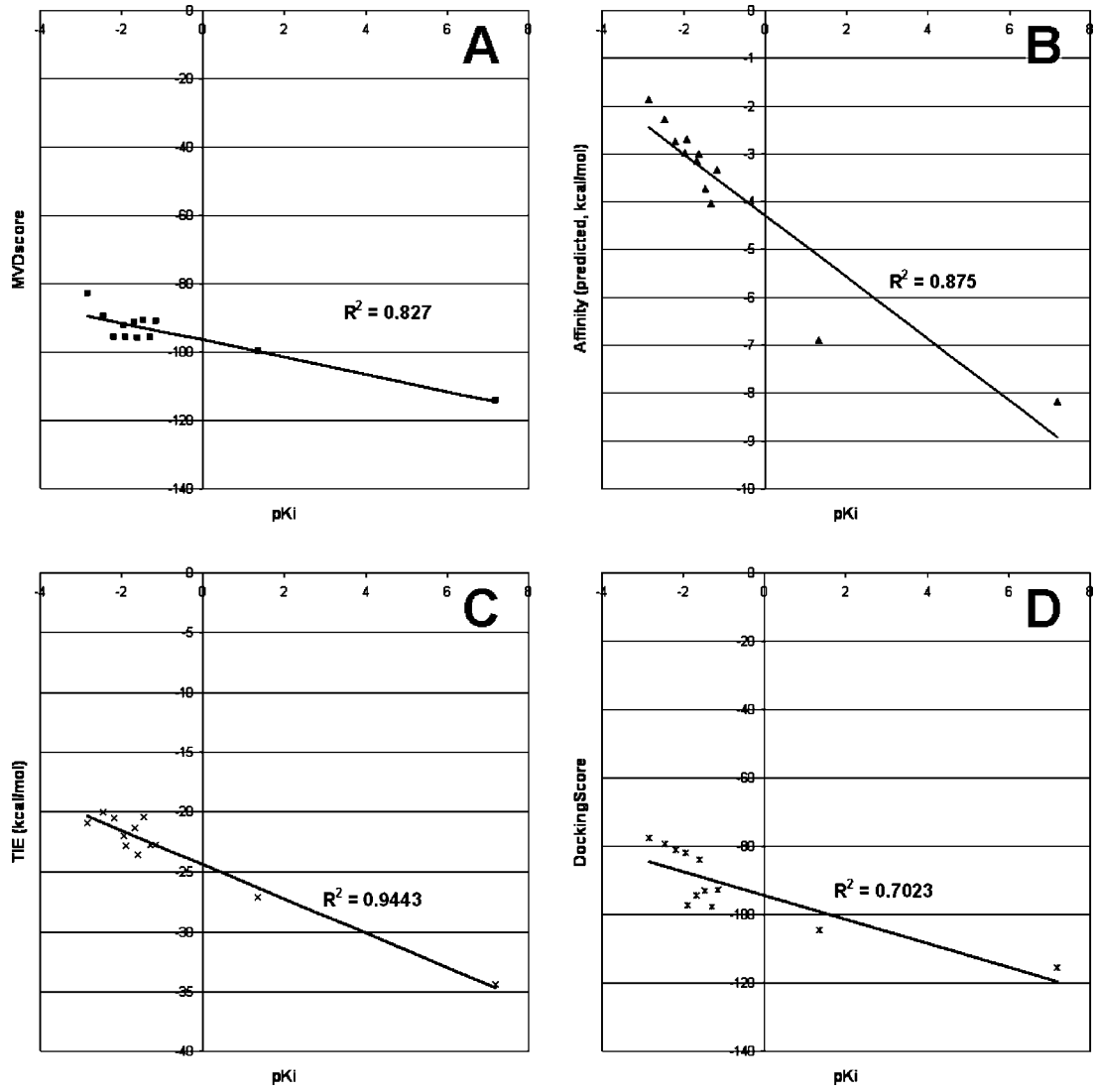

Figure 8. Scatter plots of the data derived from the MVD docking calculations and experimental pK_i values: pK_i vs (A) MVD score, $R^2 = 0.827$; (B) predicted affinity, $R^2 = 0.875$; (C) total interaction energy (TIE), $R^2 = 0.9443$; (D) docking score, $R^2 = 0.7023$.

internal coordinates space.[54] Docking took an average of 3 min/molecule on a four AMD 64-bit processors RedHat linux server with 4 GB of RAM. The speed for each compound was dependent on the number of torsional degrees of freedom.

ICM-VLS Scoring Function. Detailed information about the ICM-VLS scoring function is given by Schapira et al..[54] The ICM-VLS scoring function[85] uses the following equation and terms:

$$\text{Score} = \Delta E_{\text{IntFF}} + T\Delta S_{\text{Tor}} + \Delta E_{\text{HBond}} + \Delta E_{\text{HBDesol}} + \Delta E_{\text{SolEl}} + \Delta E_{\text{HPhob}} + Q_{\text{Size}} \quad (2)$$

where ΔE_{IntFF} accounts for the van der Waals and internal force field energy of the ligand. $T\Delta S_{\text{Tor}}$ is the change in free energy due to the conformational entropy loss of the ligand upon binding. $\Delta E_{\text{HBondis}}$ is the hydrogen bonding term, while $\Delta E_{\text{HBDesol}}$ accounts for the disruption of hydrogen bonds with solvent (desolvation of hydrogen bond donors and acceptors). ΔE_{SolEl} is the solvation electrostatic energy change upon binding. ΔE_{SolEl} was calculated using the boundary element Poisson equation solver as implemented in the REBEL[86] module of ICM. The ΔE_{HPhob} is the hydrophobic free energy gain, and Q_{Size} is a size correction term.[54]

Docking Calculations Using ICM. Compound Preparation. The compounds experimentally confirmed as thermolysin binders were used for regular docking into thermolysin. Docking calculations of the thermolysin inhibitors were performed using the ICM[87] docking module with default setup. The structures of the active compounds were energy minimized in the same environment and saved in PDB format. These energy-minimized inhibitors were then reposed into ICM and converted into ICM object, and MMFF charges[88−90] were assigned for each of the ligand.

Target Preparation. The target was prepared as described for the ICM-VLS screening.

Docking Process. The compounds were docked using the "interactive docking" menu of ICM. A stack of different docked conformations were generated and visually checked. The best docking conformations were selected on the basis of docking energies, rmsd of the ligand from the initial ligand conformation, and similarities to known X-ray crystal structures from PDB (hydrogen bonding with active site amino acids and interactions with catalytic zinc). Each ligand docking took an average of 2 min/molecule on a four AMD 64-bit processors Red Hat Linux server with 4 GB of RAM.

Calculation of Binding Free Energy. The docking conformation validated as most realistic for each compound was used for calculation the ligand−thermolysin binding energy (Cal.ΔG) using the ICM script for binding energy calculations. Cal.ΔG was compared with the experimental free energies of binding (Exp.ΔG) calculated from the experimental K_i values using eq 3.

$$\Delta G = -RT\ln K_i \quad (3)$$

Table 6. Hydrogen Bonding Interactions and Zinc Interactions of Thermolysin Inhibitors[a]

compd	interactions with Zn, if any (distance in Å)	H-bond, if any (atom no., length in Å)
2	Zn−N2 (3.15)	N2−Glu143 (OE2, 3.05) O3−His231 (NE2, 2.87) O10−Ala113 (O, 3.02) O10−Glu143 (OE2, 3.77) O21−Trp115 (N, 2.79; O, 2.92)
3	Zn−N2 (2.98)	O3−Asn112 (OD1, 2.96), Ala113 (O, 3.1) O22−Trp115 (O, 3.01)
4	Zn−N2 (2.75)	O3−Asn112 (OD, 2.95) O10−His142 (NE2, 3.04), Arg203 (NH2, 2.23) O19−Arg203 (NH2, 2.96) O20−Val139 (O, 3.33)
6	Zn−N2 ((3.29)	N2−His231 (NE2, 2.66) O3−Asn112 (OD1, 2.87; ND2, 3.12) O10−Arg203 (NH1, 3.27; NH2, 2.89) O19−Arg203 (NH2, 2.64) O23−Trp115 (O, 2.66)
7	Zn−N2 (2.88) Zn−O10 (3.05)	O3−His231 (NE2, 3.12) O10−His142 (NE2, 2.88), Arg203 (NH2, 3.54) O19−Arg203 (NH2, 2.61) O20−Glu143 (OE2, 2.9)
9		O1−Arg203 (NH1, 2.88) O7−Arg203 (NH2, 2.65)
13		O11−Arg203 (NH1, 3.19; NH2, 2.64) O12−Arg203 (NH2, 2.88)
16	Zn−O8 (3.34)	N6−Arg203 (NH1, 2.85) O8−Arg203 (NH2, 2.63)
17	Zn−N2 (2.86) Zn−O10 (3.33)	O3−Asn112 (OD1, 2.94) O10−His142 (NE2, 3.05), Arg203 (NH2, 3.01) O21−Arg203 (NH2, 2.31), Asp170 (OD1, 3.23)
19	Zn−N2 (2.75) Zn−O10 (3.57)	O3−Asn112 (OD1, 3.02) O10−Arg203 (NH2, 2.9), His142 (NE2, 3.04) O20−Val139 (O, 3.33) O21−Arg203 (NH2, 2.9)
20		O3−Asn112 (OD1, 2.9), Ala113 (O, 3.33) O20−Trp115 (O, 3.11)
21	Zn−N1 (3.34) Zn−O16 (2.98)	O4−His231 (NE2, 2.94) O13−Ala113 (O, 3.19), Glu143 (OE1, 3.11) O23−Trp115 (O, 2.62; N, 2.68)

[a] The interactions were analyzed using the most favorable docking mode of the ICM docking. Atomic numbering of the different compounds is given in Figure 1. The given atomic distances are between heavy atoms (O or N) involved in the hydrogen bond.

where R is the gas constant (0.001 98 kcal/mol) and T is the temperature (298 K).

Cal.ΔG was calculated by the ICM script utilizing eqs 4 and 5.[91]

$$\Delta G = \Delta G_{\mathrm{H}} + \Delta G_{\mathrm{EL}} + \Delta G_{\mathrm{S}} + C \tag{4}$$

$$\Delta G = \Delta G_{\mathrm{H}} + \Delta G_{\mathrm{COUL}} + \Delta G_{\mathrm{DESOLV}} + \Delta G_{\mathrm{S}} + C \tag{5}$$

where ΔG_{H} is the hydrophobic or cavity term, which accounts for the variation of water/nonwater interface area, ΔG_{EL} is the electrostatic term composed of Coulombic (ΔG_{COUL}) interactions and desolvation ($\Delta G_{\mathrm{DESOLV}}$) of partial charges transferred from an aqueous medium to a protein core environment, and ΔG_{S} is the entropic term that results from the decrease in the conformational freedom of functional groups buried upon complexation. C is a constant that accounts for entropy changes due to decreased concentration of free molecules (cratic factor) and loss of rotational/translational degrees of freedom.[91]

Docking Calculations Using Molegro Virtual Docker. Algorithm and Scoring Function. The docking module of Molegro Virtual Docker (MVD), MolDock, is based on a new heuristic search algorithm that combines differential evolution (DE) with a cavity prediction algorithm.[92] One scoring function of MolDock (MolDock Score or MVDScore) is an extension of the piecewise linear potential (PLP) originally proposed by Gehlhaar et al.[93−95] and later extended by Yang et al.[76] that includes new hydrogen bonding and electrostatic terms. To further improve docking accuracy, a reranking scoring function has been introduced that identifies the most promising docking solution from the solutions obtained by the docking algorithm.[92]

The docking scoring function, E_{score} (Docking Score), which is another scoring function of MVD, is defined by the following energy terms.

$$E_{\mathrm{score}} = E_{\mathrm{inter}} + E_{\mathrm{intra}} \tag{6}$$

E_{inter} is the ligand−protein interaction energy calculated by

$$E_{\mathrm{inter}} = \sum_{i \in \text{ligand}} \sum_{j \in \text{protein}} \left[E_{\mathrm{PLP}}(r_{ij}) + 332.0 \frac{q_i q_j}{4 r_{ij}^{\,2}} \right] \tag{7}$$

The summation runs over all heavy atoms in the ligand and in the protein, including any cofactor atoms (here, calcium and zinc ions) and water molecule atoms that might be present (all water molecules were removed in the present docking study).[92] E_{PLP} is a "piecewise linear potential" using two different sets of parameters: one set for approximating the steric (van der Waals) term between atoms and another set approximating a stronger potential for hydrogen bonds. The linear potential is defined by the following functional form:

$$E_{\mathrm{PLP}}(0) = A_0, \quad E_{\mathrm{PLP}}(R_1) = 0, \quad E_{\mathrm{PLP}}(R_2) = E_{\mathrm{PLP}}(R_3) = A_1, \quad E_{\mathrm{PLP}}(r) = 0 \quad \text{for} \quad r \geq \mathrm{R4} \tag{8}$$

and is linearly interpolated between these values.[96]

The second term describes the electrostatic interactions between charged atoms. It is a Coulomb potential with a distance dependent dielectric constant given by $D(r) = 4r$. The numerical value of 332.0 fixes the units of the electrostatic energy to kcal/mol.

E_{intra} is the intramolecular energy of the ligand calculated by

$$E_{\mathrm{intra}} = \sum_{i \in \text{ligand}} \sum_{j \in \text{ligand}} E_{\mathrm{PLP}}(r_{ij}) + \sum_{\text{flexible bonds}} A[1 - \cos(m\theta - \theta_0)] + E_{\mathrm{clash}} \tag{9}$$

The double summation is between all atom pairs in the ligand excluding atom pairs connected by two bonds or less. The second term is a torsional energy term, parametrized according to hybridization of bonded atoms, while θ is the torsional angle of the bond. An average of torsional energy bond contribution is used if several torsions can be determined between bonded atoms. The last term, E_{clash}, assigns a penalty of 1000 if the distance between two heavy atoms (more than two bonds apart) is less than 2.0 Å. Thus, E_{clash} term punishes infeasible ligand conformations.[92,96]

Docking Search Algorithm. The docking search algorithm (MolDock Optimizer) used by MolDock is based on an evolutionary algorithm.[97,98] Evolutionary algorithms are iterative optimization techniques inspired by Darwinian evolution theory.[99] MolDock Optimizer is based on an evolutionary algorithm variant called differential evolution. The differential evolution algorithm was introduced by Storn and Price in 1995.[100] Compared to more widely known evolutionary algorithm techniques (e.g., GA, evolutionary programming, and evolution strategies), differential evolution uses a different approach to select and modify candidate solutions.[99]

Stepwise Docking Method. Active compounds and thermolysin (PDB code 1gxw) was uploaded without water molecules. When necessary, bonds, bond orders, hybridizations, and hydrogen atoms

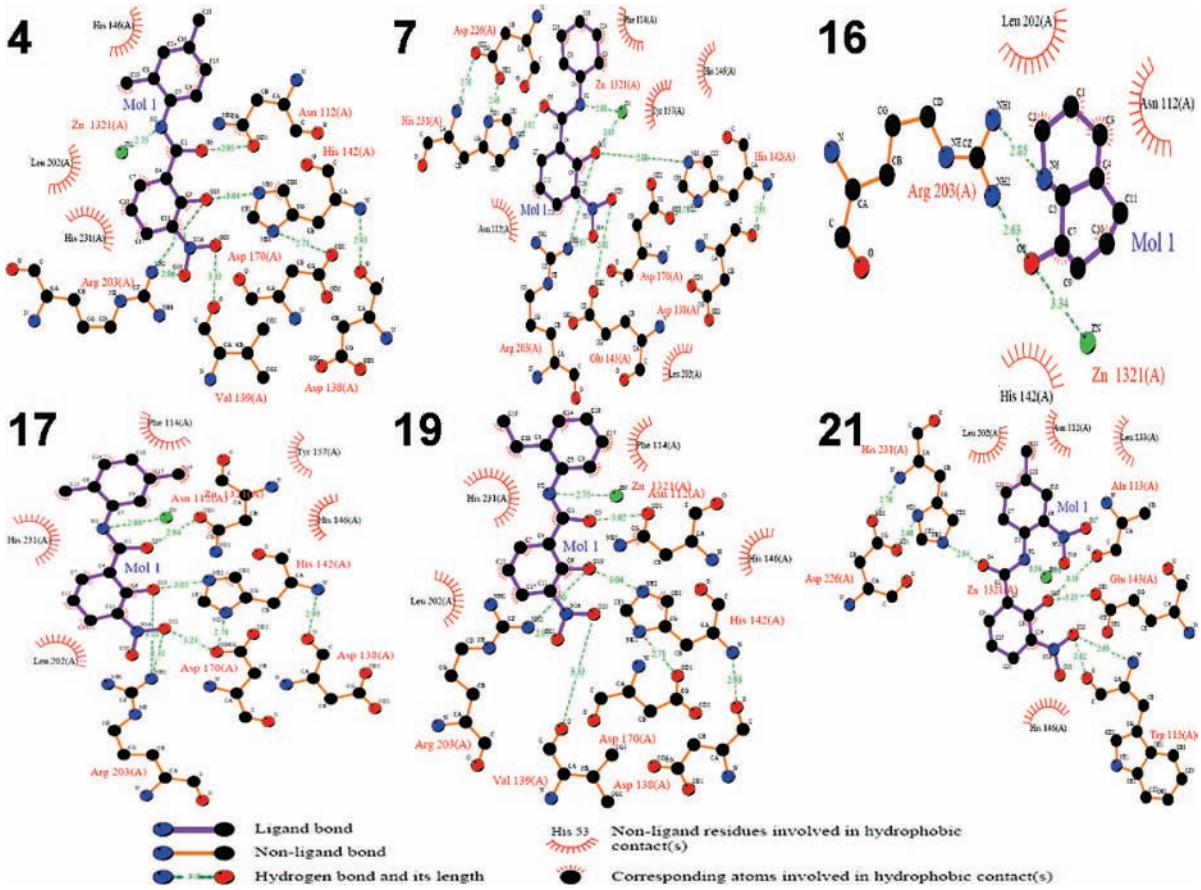

Figure 9. Molecular interactions between the active site of thermolysin and compounds **4**, **7**, **16**, **17**, **19**, and **21**. The illustration was generated with LigPlot.[74]

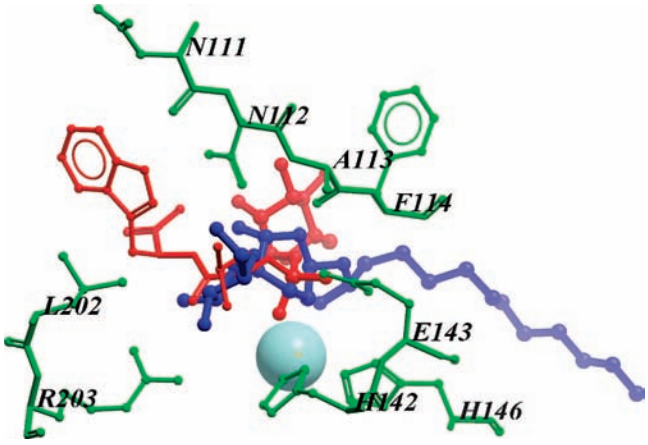

Figure 10. Superimposition of compound **9** (blue) and the inhibitor *N*-phosphoryl-L-leucinamide (red) from the X-ray crystal structure complex 1tlp.[75] These ligands are relatively different but share some structural features. The most important amino acids for ligand binding are shown in green. The zinc atom is shown as blue CPK model.

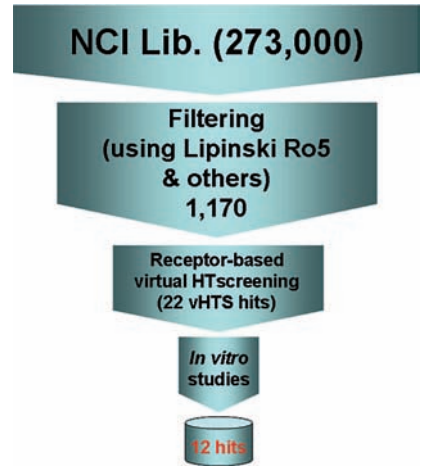

Figure 11. Flow diagram for the virtual high-throughput screening (vHTS) using ICM-VLS module.

were added, charges were assigned (a formal charge of +2 for Zn ion),[92] and flexible torsions of ligands were detected. Then an automatic procedure was used to detect possible binding cavities. During this process the maximum number of cavities was fixed to 5, the grid resolution was 0.80 Å, and probe size was 1.2 Å, while other parameters were default. Two cavities were detected, and the cavity around the catalytic zinc ion (volume of approximately 70−72 Å^3) was used for docking calculations using MolDock Optimizer as search algorithm. During docking the grid resolution was set to 0.3 Å, while the binding site radius was set to 21 Å. The best ligand poses were chosen on the basis of visual inspection of the interactions at the active site using the same criteria as for the ICM docking.

The docking calculations were performed with a dual processor Windows XP based computer with 2 GB of RAM, and each docking process took 5−7 min.

Scorings Generated by MVD. In addition to MVDscore and DockingScore (E_{score}, explained in equations), the following MVD based scores were also calculated for each compound:

(1) Affinity calculated by MVD in kJ/mol (converted to kcal/mol for easy comparisons).

(2) ReRank. To further increase the docking accuracy, the 10 solutions obtained from the 10 independent docking runs were

reranked using a more complex scoring function.[92] In addition to the docking scoring function terms, an sp^2-sp^2 torsion term and a Lennard-Jones 12−6 potential[101] are included.

(3) TIE, which should correspond to total interaction energy between ligand and target.

(4) HBond, the hydrogen bonding energy between ligand and target.

(5) LE1, ligand efficiency 1, which corresponds to MolDock Scores divided by the number of heavy atoms.

(6) LE2, ligand efficiency 2, which corresponds to the affinity divided by the number of heavy atoms.

Data Plotting and Regression Analysis. For easy interpretations of the interactions between the thermolysin and the compounds, LigPlot[74] was used to construct schematic 2D plots of the interactions. Regression analysis of different data derived from experiments and docking calculations were performed by MS Excel. For the kinetic experiments, the Enzyme Kinetic module of SigmaPlot, version 10, integrated with SigmaStat was used.

Analysis of the Purity of the Compounds. The purity of the NCI compounds was analyzed by tandem MS.

Chemicals. Formic acid was supplied by Fluka (Steinheim, Germany), and LC−MS grade methanol and water were supplied by Riedel-de-Haën (Seelze, Germany) and were used as mobile phase.

Method and Equipment. Stock solutions of the different compounds were diluted to 1 μM with 50% methanol in 5 mmol/L aqueous formic acid.

A triple quadruple mass spectrometer (Quattro Premier XE benchtop tandem quadruple mass spectrometer from Waters, Manchester, U.K.) fitted with a Z-spray ion source was used. The mass spectrometer was operated in both positive and negative electrospray ion (ESI) modes, and spray voltage was 3.0 kV. The system was controlled by MassLynx, version 4.1, software. Parameters were as follows: desolvation gas temperature, 260 °C; source temperature, 120 °C; desolvation gas flow, 300 L/h; cone gas flow, 40 L/h; collision gas pressure, 3.5×10^{-3} mbar (argon); ion energies, 0.9 V for both quadruples. Diluted samples (1 μM) were infused into the ionization probe using a syringe pump at a flow rate of 10.0 μL/min. After optimum cone voltage and collision energy were found for parent ion and most of the abundant daughter ions produced from the fragmentation of parent, MS/MS spectra were acquired.

Acknowledgment. We are grateful to University of Tromsø for providing funding for this research and also to the Drug Synthesis and Chemistry Branch, DTP, Division of Cancer Treatment and Diagnosis, NCI, for providing us the VLS hit compounds. We are also thankful to Dr. René Thomsen and to Molegro ApS, Denmark, for giving us the possibility of using the trial version of MVD. M.T.H.K. and I.S. conceived and designed the work. M.T.H.K. performed the VLS, in vitro experiments, data analysis, molecular docking studies, and wrote the first draft of the manuscript. O.-M.F. performed the tandem-MS analysis. I.S. analyzed the data and the manuscript and arranged the funding.

Supporting Information Available: Purity data (tandem-MS spectra) of the individual active compounds. This material is available free of charge via the Internet at http://pubs.acs.org.

References

(1) Latt, S. A.; Holmquist, B.; Vallee, B. L. Thermolysin: a zinc metalloenzyme. *Biochem. Biophys. Res. Commun.* **1969**, *37* (2), 333–339.

(2) Feder, J.; Garrett, L. R.; Wildi, B. S. Studies on the role of calcium in thermolysin. *Biochemistry* **1971**, *10* (24), 4552–4556.

(3) Morihara, K.; Tsuzuki, H. Thermolysin: kinetic study with oligopeptides. *Eur. J. Biochem.* **1970**, *15* (2), 374–380.

(4) Inouye, K.; Lee, S. B.; Tonomura, B. Effect of amino acid residues at the cleavable site of substrates on the remarkable activation of thermolysin by salts. *Biochem. J.* **1996**, *315* (Part 1), 133–138.

(5) Jin, F.; Matsushita, O.; Katayama, S.; Jin, S.; Matsushita, C.; Minami, J.; Okabe, A. Purification, characterization, and primary structure of *Clostridium perfringens* lambda-toxin, a thermolysin-like metalloprotease. *Infect. Immun.* **1996**, *64* (1), 230–237.

(6) Mariencheck, W. I.; Alcorn, J. F.; Palmer, S. M.; Wright, J. R. *Pseudomonas aeruginosa* elastase degrades surfactant proteins A and D. *Am. J. Respir. Cell Mol. Biol.* **2003**, *28* (4), 528–537.

(7) Hobden, J. A. *Pseudomonas aeruginosa* proteases and corneal virulence. *DNA Cell Biol* **2002**, *21* (5−6), 391–396.

(8) Naka, A.; Yamamoto, K.; Miwatani, T.; Honda, T. Characterization of two forms of hemagglutinin/protease produced by *Vibrio cholerae* non-O1. *FEMS Microbiol. Lett.* **1992**, *77* (1−3), 197–200.

(9) Schmidtchen, A.; Holst, E.; Tapper, H.; Bjorck, L. Elastase-producing *Pseudomonas aeruginosa* degrade plasma proteins and extracellular products of human skin and fibroblasts, and inhibit fibroblast growth. *Microb. Pathog.* **2003**, *34* (1), 47–55.

(10) Schmidtchen, A.; Wolff, H.; Rydengard, V.; Hansson, C. Detection of serine proteases secreted by *Lucilia sericata* in vitro and during treatment of a chronic leg ulcer. *Acta Derm.-Venereol.* **2003**, *83* (4), 310–311.

(11) Smith, A. W.; Chahal, B.; French, G. L. The human gastric pathogen *Helicobacter pylori* has a gene encoding an enzyme first classified as a mucinase in *Vibrio cholerae*. *Mol. Microbiol.* **1994**, *13* (1), 153–160.

(12) Altincicek, B.; Linder, M.; Linder, D.; Preissner, K. T.; Vilcinskas, A. Microbial metalloproteinases mediate sensing of invading pathogens and activate innate immune responses in the lepidopteran model host *Galleria mellonella*. *Infect. Immun.* **2007**, *75* (1), 175–183.

(13) Hung, C. Y.; Seshan, K. R.; Yu, J. J.; Schaller, R.; Xue, J.; Basrur, V.; Gardner, M. J.; Cole, G. T. A metalloproteinase of *Coccidioides posadasii* contributes to evasion of host detection. *Infect. Immun.* **2005**, *73* (10), 6689–6703.

(14) Miyoshi, S.-I.; Sinoda, S. Microbial metalloproteases and pathogenesis. *Microbes Infect.* **2000**, *2*, 91–98.

(15) Miyoshi, S.-I.; Nakazawa, H.; Kawata, K.; Tomochika, K. I.; Tobe, K.; Shinoda, S. Characterization of the hemorrhagic reaction caused by *Vibrio vulnificus* metalloproteinase, a member of the thermolysin family. *Infect. Immun.* **1998**, *66*, 4851–4855.

(16) Miyoshi, S.; Sonoda, Y.; Wakiyama, H.; Rahman, M. M.; Tomochika, K.; Shinoda, S.; Yamamoto, S.; Tobe, K. An exocellular thermolysin-like metalloprotease produced by *Vibrio fluvialis*: purification, characterization, and gene cloning. *Microb. Pathog.* **2002**, *33* (3), 127–134.

(17) Vilcinskas, A.; Wedde, M. Insect inhibitors of metalloproteinases. *IUBMB Life* **2002**, *54* (6), 339–343.

(18) Supuran, C.; Scozzafava, A.; Mastrolorenzo, A. Bacterial proteases: current therapeutic use and future prospects for the development of new antibiotics. *Expert Opin. Ther. Pat.* **2001**, *11*, 221–259.

(19) Travis, J.; Potempa, J. Bacterial proteinases as targets for the development of second-generation antibiotics. *Biochim. Biophys. Acta* **2000**, *1477* (1−2), 35–50.

(20) Roques, B. P. Zinc metallopeptidases: active site structure and design of selective and mixed inhibitors: new approaches in the search for analgesics and anti-hypertensives. *Biochem. Soc. Trans.* **1993**, *21* (3, Part 3), 678–85.

(21) Roques, B. P.; Noble, F.; Dauge, V.; Fournie-Zaluski, M. C.; Beaumont, A. Neutral endopeptidase 24.11: structure, inhibition, and experimental and clinical pharmacology. *Pharmacol Rev* **1993**, *45* (1), 87–146.

(22) Wyvratt, M. J.; Patchett, A. A. Recent developments in the design of angiotensin-converting enzyme inhibitors. *Med. Res. Rev.* **1985**, *5* (4), 483–531.

(23) Gomez-Monterrey, I.; Beaumont, A.; Nemecek, P.; Roques, B. P.; Fournie-Zaluski, M. C. New thiol inhibitors of neutral endopeptidase EC 3.4.24.11: synthesis and enzyme active-site recognition. *J. Med. Chem.* **1994**, *37* (12), 1865–1873.

(24) Holmes, M. A.; Matthews, B. W. Structure of thermolysin refined at 1.6 Å resolution. *J. Mol. Biol.* **1982**, *160* (4), 623–639.

(25) Tiraboschi, G.; Jullian, N.; Thery, V.; Antonczak, S.; Fournie-Zaluski, M. C.; Roques, B. P. A three-dimensional construction of the active site (region 507−749) of human neutral endopeptidase (EC.3.4.24.11). *Protein Eng.* **1999**, *12* (2), 141–149.

(26) Bohacek, R. S.; McMartin, C.; Guida, W. C. The art and practice of structure-based drug design: a molecular modeling perspective. *Med. Res. Rev.* **1996**, *16* (1), 3–50.

(27) Turner, A. J.; Isaac, R. E.; Coates, D. The neprilysin (NEP) family of zinc metalloendopeptidases: genomics and function. *BioEssays* **2001**, *23* (3), 261–9.

(28) Guido, R. V.; Oliva, G.; Andricopulo, A. D. Virtual screening and its integration with modern drug design technologies. *Curr. Med. Chem.* **2008**, *15* (1), 37–46.

(29) Rollinger, J. M.; Stuppner, H.; Langer, T. Virtual screening for the discovery of bioactive natural products. *Prog. Drug Res.* **2008**, *65*, 211, 213–249.
(30) Alex, A. A.; Flocco, M. M. Fragment-based drug discovery: what has it achieved so far? *Curr. Top. Med. Chem.* **2007**, *7* (16), 1544–1567.
(31) Cavasotto, C. N.; Orry, A. J. Ligand docking and structure-based virtual screening in drug discovery. *Curr. Top. Med. Chem.* **2007**, *7* (10), 1006–1014.
(32) Dubinina, G. G.; Chupryna, O. O.; Platonov, M. O.; Borisko, P. O.; Ostrovska, G. V.; Tolmachov, A. O.; Shtil, A. A. In silico design of protein kinase inhibitors: successes and failures. *Anticancer Agents Med. Chem.* **2007**, *7* (2), 171–188.
(33) Ekins, S.; Mestres, J.; Testa, B. In silico pharmacology for drug discovery: methods for virtual ligand screening and profiling. *Br. J. Pharmacol.* **2007**, *152* (1), 9–20.
(34) Ekins, S.; Mestres, J.; Testa, B. In silico pharmacology for drug discovery: applications to targets and beyond. *Br. J. Pharmacol.* **2007**, *152* (1), 21–37.
(35) Geromichalos, G. D. Importance of molecular computer modeling in anticancer drug development. *J. BUON* **2007**, *12* (Suppl. 1), S101–S118.
(36) Glicksman, M. A.; Cuny, G. D.; Liu, M.; Dobson, B.; Auerbach, K.; Stein, R. L.; Kosik, K. S. New approaches to the discovery of cdk5 inhibitors. *Curr. Alzheimer Res.* **2007**, *4* (5), 547–549.
(37) Hirayama, N. Docking method for drug discovery. *Yakugaku Zasshi* **2007**, *127* (1), 113–122.
(38) Hirokawa, T. Receptor−ligand docking simulation for membrane proteins. *Yakugaku Zasshi* **2007**, *127* (1), 123–131.
(39) Lennernas, H. Animal data: the contributions of the Ussing chamber and perfusion systems to predicting human oral drug delivery in vivo. *Adv Drug Delivery Rev.* **2007**, *59* (11), 1103–1120.
(40) McInnes, C. Virtual screening strategies in drug discovery. *Curr. Opin. Chem. Biol.* **2007**, *11* (5), 494–502.
(41) Pirard, B. Insight into the structural determinants for selective inhibition of matrix metalloproteinases. *Drug Discovery Today* **2007**, *12* (15−16), 640–646.
(42) Reddy, A. S.; Pati, S. P.; Kumar, P. P.; Pradeep, H. N.; Sastry, G. N. Virtual screening in drug discovery−a computational perspective. *Curr. Protein Pept. Sci.* **2007**, *8* (4), 329–351.
(43) Naskanishi, K.; Matsuno, R. Continuous peptide synthesis in a water-immisicible organic solvent with an immobilized enzyme. *Ann. N.Y. Acad. Sci.* **1990**, *613*, 652–655.
(44) Veljkovic, V.; Veljkovic, N.; Este, J. A.; Huther, A.; Dietrich, U. Application of the EIIP/ISM bioinformatics concept in development of new drugs. *Curr. Med. Chem.* **2007**, *14* (4), 441–453.
(45) Villoutreix, B. O.; Renault, N.; Lagorce, D.; Sperandio, O.; Montes, M.; Miteva, M. A. Free resources to assist structure-based virtual ligand screening experiments. *Curr. Protein Pept. Sci.* **2007**, *8* (4), 381–411.
(46) Yoon, S.; Smellie, A.; Hartsough, D.; Filikov, A. Surrogate docking: structure-based virtual screening at high throughput speed. *J. Comput.-Aided Mol. Des.* **2005**, *19* (7), 483–497.
(47) Plewczynski, D.; Hoffmann, M.; von Grotthuss, M.; Ginalski, K.; Rychewski, L. In silico prediction of SARS protease inhibitors by virtual high throughput screening. *Chem. Biol. Drug Des.* **2007**, *69* (4), 269–279.
(48) Chen, H.; Lyne, P. D.; Giordanetto, F.; Lovell, T.; Li, J. On evaluating molecular-docking methods for pose prediction and enrichment factors. *J. Chem. Inf. Model.* **2006**, *46* (1), 401–415.
(49) Prathipati, P.; Saxena, A. K. Evaluation of binary QSAR models derived from LUDI and MOE scoring functions for structure based virtual screening. *J. Chem. Inf. Model.* **2006**, *46* (1), 39–51.
(50) Maiorov, V.; Sheridan, R. P. Enhanced virtual screening by combined use of two docking methods: getting the most on a limited budget. *J. Chem. Inf. Model.* **2005**, *45* (4), 1017–1023.
(51) Perola, E.; Walters, W. P.; Charifson, P. S. A detailed comparison of current docking and scoring methods on systems of pharmaceutical relevance. *Proteins* **2004**, *56* (2), 235–249.
(52) Bursulaya, B. D.; Totrov, M.; Abagyan, R.; Brooks, C. L., 3rd. Comparative study of several algorithms for flexible ligand docking. *J. Comput.-Aided Mol. Des.* **2003**, *17* (11), 755–763.
(53) Cavasotto, C. N.; Abagyan, R. A. Protein flexibility in ligand docking and virtual screening to protein kinases. *J. Mol. Biol.* **2004**, *337* (1), 209–225.
(54) Schapira, M.; Abagyan, R.; Totrov, M. Nuclear hormone receptor targeted virtual screening. *J. Med. Chem.* **2003**, *46* (14), 3045–3059.
(55) Lipinski, C. A. Chris Lipinski discusses life and chemistry after the rule of five. *Drug Discovery Today* **2003**, *8* (1), 12–16.
(56) Miller, R. E.; Reid, W. A., Jr. *Schistosoma mansoni*: salicylanilides as topical prophylactic against cercarial penetration of mice. *Exp. Parasitol.* **1986**, *61* (3), 359–368.
(57) Marking, L. L.; Willford, W. A. *Comparative Toxicity of 29 Nitrosalicylanilides and Related Compounds to Eight Species of Fish*; USGS: Reston, VA, 1970.
(58) Chen, S.-T.; Kan, P.-C.; Chein, I.-F.; Hu, Y.-C. Chemotherapy of schistosomiasis. Synthesis of substituted salicylanilides and benzimidazole derivatives. *Yaoxue Xuebao* **1963**, *10* (11), 683–687.
(59) Jadhav, G. V.; Nerlekar, P. G. Bromination of compounds containing two aromatic nuclei. XI. Bromination of arylamides of 3-nitrosalicyclic acid. *J. Univ. Bombay, Sci.: Phys. Sci. Math. Biol. Sci. Med.* **1951**, *20* (Part 3, Science No. 30), 97–100.
(60) Aoshima, M.; Tsukagoshi, S.; Sakurai, Y.; Oh-ishi, J.; Ishida, T.; Kobayashi, H. Antitumor activities of newly synthesized *N*4-acyl-1-beta-D-arabinofuranosylcytosine. *Cancer Res.* **1976**, *36* (8), 2726–2732.
(61) Royals, E. E. Isomeric citrylideneacetic acids. *J. Am. Chem. Soc.* **1947**, *69*, 841–844.
(62) Ujiie, T.; Koshimura, S. Action mechanism of 2-(2-hydroxy-5-*n*-hexylphenyl)-8-quinolinol-4-carboxylic acid−with special reference to selective inhibition of DNA synthesis in ascites hepatoma AH 13 cells in culture. *Chem. Pharm. Bull. (Tokyo)* **1975**, *23* (1), 72–81.
(63) Lee, M. S.; Keith, C.; Auspitz, B. A.; Zimmermann, G. R.; Nichols, M. J.; Foley, M. A. Methods for the Treatment of Neoplasms. WO/2004/006906, 2004.
(64) Abagyan, R.; Totrov, M. High-throughput docking for lead generation. *Curr. Opin. Chem. Biol.* **2001**, *5* (4), 375–382.
(65) Cheng, Y.; Prusoff, W. H. Relationship between the inhibition constant (K1) and the concentration of inhibitor which causes 50% inhibition (I50) of an enzymatic reaction. *Biochem. Pharmacol.* **1973**, *22* (23), 3099–3108.
(66) Gaucher, J. F.; Selkti, M.; Tiraboschi, G.; Prange, T.; Roques, B. P.; Tomas, A.; Fournie-Zaluski, M. C. Crystal structures of alpha-mercaptoacyldipeptides in the thermolysin active site: structural parameters for a Zn monodentation or bidentation in metalloendopeptidases. *Biochemistry* **1999**, *38* (39), 12569–12576.
(67) Selkti, M.; Tomas, A.; Gaucher, J. F.; Prange, T.; Fournie-Zaluski, M. C.; Chen, H.; Roques, B. P. Interactions of a new alpha-aminophosphinic derivative inside the active site of TLN (thermolysin): a model for zinc-metalloendopeptidase inhibition. *Acta Crystallogr., Sect. D: Biol. Crystallogr.* **2003**, *59* (Part 7), 1200–1205.
(68) Bartlett, P. A.; Marlowe, C. K. Possible role for water dissociation in the slow binding of phosphorus-containing transition-state-analogue inhibitors of thermolysin. *Biochemistry* **1987**, *26* (26), 8553–8561.
(69) Holden, H. M.; Tronrud, D. E.; Monzingo, A. F.; Weaver, L. H.; Matthews, B. W. Slow- and fast-binding inhibitors of thermolysin display different modes of binding: crystallographic analysis of extended phosphonamidate transition-state analogues. *Biochemistry* **1987**, *26* (26), 8542–8553.
(70) Kitagishi, K.; Hiromi, K. Binding between thermolysin and its specific inhibitor, *N*-phosphoryl-L-leucyl-L-tryptophan (PLT). *J. Biochem.* **1986**, *99* (1), 191–197.
(71) Wolfenden, R. Transition state analog inhibitors and enzyme catalysis. *Annu. Rev. Biophys. Bioeng.* **1976**, *5*, 271–306.
(72) Frieden, C.; Kurz, L. C.; Gilbert, H. R. Adenosine deaminase and adenylate deaminase: comparative kinetic studies with transition state and ground state analogue inhibitors. *Biochemistry* **1980**, *19* (23), 5303–5309.
(73) Morrison, J. F.; Walsh, C. T. The behavior and significance of slow-binding enzyme inhibitors. *Adv. Enzymol. Relat. Areas Mol. Biol.* **1988**, *61*, 201–301.
(74) Wallace, A. C.; Laskowski, R. A.; Thornton, J. M. LIGPLOT: a program to generate schematic diagrams of protein−ligand interactions. *Protein Eng.* **1995**, *8* (2), 127–134.
(75) Tronrud, D. E.; Monzingo, A. F.; Matthews, B. W. Crystallographic structural analysis of phosphoramidates as inhibitors and transition-state analogs of thermolysin. *Eur. J. Biochem.* **1986**, *157* (2), 261–268.
(76) Lee, H. S.; Choi, J.; Kufareva, I.; Abagyan, R.; Filikov, A.; Yang, Y.; Yoon, S. Optimization of high throughput virtual screening by combining shape-matching and docking methods. *J. Chem. Inf. Model.* **2008**, *48* (3), 489–497.
(77) Klebe, G. Virtual ligand screening: strategies, perspectives and limitations. *Drug Discovery Today* **2006**, *11* (13−14), 580–594.
(78) Carlson, H. A. Protein flexibility and drug design: how to hit a moving target. *Curr. Opin. Chem. Biol.* **2002**, *6* (4), 447–452.
(79) Carlson, H. A. Protein flexibility is an important component of structure-based drug discovery. *Curr. Pharm. Des.* **2002**, *8* (17), 1571–1578.
(80) Feder, J.; Schuck, J. M. Studies on the *Bacillus subtilis* neutral-protease- and *Bacillus thermoproteolyticus* thermolysin-catalyzed hydrolysis of dipeptide substrates. *Biochemistry* **1970**, *9* (14), 2784–2791.
(81) Gaucher, J. F.; Selkti, M.; Prange, T.; Tomas, A. The 2.2 Å resolution structure of thermolysin (TLN) crystallized in the presence of

potassium thiocyanate. *Acta Crystallogr., Sect. D: Biol. Crystallogr.* **2002**, *58* (Part 12), 2198–2200.
(82) Totrov, M.; Abagyan, R. Protein−Ligand Docking as an Energy Optimization Problem. In *Drug−Receptor Thermodynamics: Introduction and Applications*; Raffa, R. B., Ed.; John Wiley & Sons: New York, 2001; pp 603−624.
(83) Schapira, M.; Raaka, B. M.; Samuels, H. H.; Abagyan, R. Rational discovery of novel nuclear hormone receptor antagonists. *Proc. Natl. Acad. Sci. U.S.A.* **2000**, *97* (3), 1008–1013.
(84) *ICM 3.4 Manual*; Molsoft LLC: San Diego, CA; www.molsoft.com.
(85) Totrov, M.; Abagyan, R. *Derivation of Sensitive Discrimination Potential for Virtual Ligand Screening*, RECOMB '99: Third Annual International Conference on Computational Molecular Biology, Lyon, France, April 11−14, 1999; Istrail, S., Pevzner, P., Waterman, M., Eds.; Association for Computing Machinery, New York: Lyon, France, 1999.
(86) Totrov, M.; Abagyan, R. Rapid boundary element solvation electrostatics calculations in folding simulations: successful folding of a 23-residue peptide. *Biopolymers* **2001**, *60* (2), 124–133.
(87) Totrov, M.; Abagyan, R. Flexible protein−ligand docking by global energy optimization in internal coordinates. *Proteins* **1997**, (Suppl. 1), 215–220.
(88) Cherkasov, A.; Shi, Z.; Li, Y.; Jones, S. J.; Fallahi, M.; Hammond, G. L. "Inductive" charges on atoms in proteins: comparative docking with the extended steroid benchmark set and discovery of a novel SHBG ligand. *J. Chem. Inf. Model.* **2005**, *45* (6), 1842–1853.
(89) Tsai, K. C.; Wang, S. H.; Hsiao, N. W.; Li, M.; Wang, B. The effect of different electrostatic potentials on docking accuracy: a case study using DOCK5.4. *Bioorg. Med. Chem. Lett.* **2008**, *18* (12), 3509–3512.
(90) Wang, J.; Wolf, R. M.; Caldwell, J. W.; Kollman, P. A.; Case, D. A. Development and testing of a general amber force field. *J. Comput. Chem.* **2004**, *25* (9), 1157–1174.
(91) Schapira, M.; Totrov, M.; Abagyan, R. Prediction of the binding energy for small molecules, peptides and proteins. *J. Mol. Recognit.* **1999**, *12*, 177–190.
(92) Thomsen, R.; Christensen, M. H. MolDock: a new technique for high-accuracy molecular docking. *J. Med. Chem.* **2006**, *49* (11), 3315–3321.
(93) Gehlhaar, D. K.; Verkhivker, G.; Rejto, P. A.; Fogel, D. B.; Fogel, L. J.; Freer, S. T. Docking Conformationally Flexible Small Molecules Into a Protein Binding Site Through Evolutionary Programming. In *Evolutionary Programming IV*, Proceedings of the Fourth Annual Conference on Evolutionary Programming; MIT Press: Cambridge, MA, 1995; pp 615−627.
(94) Gehlhaar, D. K.; Verkhivker, G. M.; Rejto, P. A.; Sherman, C. J.; Fogel, D. B.; Fogel, L. J.; Freer, S. T. Molecular recognition of the inhibitor AG-1343 by HIV-1 protease: conformationally flexible docking by evolutionary programming. *Chem. Biol.* **1995**, *2* (5), 317–324.
(95) Gehlhaar, D. K.; Bouzida, D.; Rejto, P. A. Fully Automated and Rapid Flexible Docking of Inhibitors Covalently Bound to Serine Proteases. In *Evolutionary Programming VII*, Proceedings of the Seventh International Conference on Evolutionary Programming; Springer: Berlin, 1998; pp 449−461.
(96) *Molegro Virtual Docker: Docking Scoring Function. User Manual*, version 2.2; Molegro: Aarhus, Denmark, 2007; Appendix I.
(97) Michalewicz, Z. *Genetic Algorithms + Data Structures = Evolution Programs*; Springer-Verlag: Berlin, 1992.
(98) Michalewicz, Z.; Fogel, D. B. *How To Solve It: Modern Heuristics*; Springer-Verlag: Berlin, 2000.
(99) *Molegro Virtual Docker: Docking Search Algorithm. User Manual*, version 2.2; Molegro: Aarhus, Denmark, 2007; Appendix II.
(100) Storn, R.; Price, K. *Differential Evolution. A Simple and Efficient Adaptive Scheme for Global Optimization over Continuous Spaces*; International Computer Science Institute: Berkley, CA, 1995.
(101) Morris, G. M.; Goodsell, D. S.; Halliday, R. S.; Huey, R.; Hart, W. E.; Belew, R. K.; Olson, A. J. Automated docking using a Lamarckian genetic algorithm and an empirical binding free energy function. *J. Comput. Chem.* **1998**, *19*, 1639–1662.

JM8008019